

ZOOM BETTER TO SEE CLEARER: HUMAN PART SEGMENTATION WITH AUTO ZOOM NET

Fangting Xia, Peng Wang, Liang-Chieh Chen & Alan L. Yuille

University of California, Los Angeles

{sukixia, jerrykingpku, lcchen, yuille}@ucla.edu

ABSTRACT

Parsing human regions into semantic parts, *e.g.*, body, head and arms *etc.*, from a random natural image is challenging while fundamental for computer vision and widely applicable in industry. One major difficulty to handle such a problem is the high flexibility of scale and location of a human instance and its corresponding parts, making the parsing task either lack of boundary details or suffer from local confusions. To tackle such problems, in this work, we propose the “Auto-Zoom Net” (AZN) for human part parsing, which is a unified fully convolutional neural network structure that: (1) parses each human instance into detailed parts. (2) predicts the locations and scales of human instances and their corresponding parts. In our unified network, the two tasks are mutually beneficial. The score maps obtained for parsing help estimate the locations and scales for human instances and their parts. With the predicted locations and scales, our model “zooms” the region into a right scale to further refine the parsing. In practice, we perform the two tasks iteratively so that detailed human parts are gradually recovered. We conduct extensive experiments over the challenging PASCAL-Person-Part segmentation, and show our approach significantly outperforms the state-of-art parsing techniques especially for instances and parts at small scale.

1 INTRODUCTION

Looking at natural images, we can easily locate the regions containing human instances, and further parse each human instance into semantic parts to estimate their poses. This provides us with understanding of the semantic actions of others in order to interact with the environments. Thus for computer vision, decomposing a human segment into detailed parts is also essential for generating real understanding of the human in an image. In addition, human parsing can be widely applicable to other computer vision tasks, *e.g.*, segmentation (Eslami & Williams, 2012; Wang et al., 2015a), pose estimation (Dong et al., 2014), fine-grained recognition (Zhang et al., 2014), and industry applications such as robotics and image descriptions for the blind.

In the literature of semantic parsing, while object-level segmentation over multiple object categories has been extensively studied along with the growing popularity of standard evaluation benchmarks such as PASCAL VOC (Everingham et al., 2014) and MS-COCO (Lin et al., 2014), human parsing (*i.e.*, segmenting human into its semantic parts) is mostly addressed under constrained conditions such as presumably accurate localization, clear appearances, or relatively simple poses, *e.g.*, (Bo & Fowlkes, 2011; Zhu et al., 2011; Eslami & Williams, 2012; Yamaguchi et al., 2012; Dong et al., 2014; Liu et al., 2015a). One of the major technique hurdles ahead to extending this detailed parsing to natural wild scenarios like the PASCAL images is the high flexibility of poses, locations, and scales of human instances and their corresponding parts, where instances can have blurry edges, difficult poses, truncated or occluded parts. This makes infeasible the traditional methods which perform well under the constrained environment.

Recently, with the rise of the powerful end-to-end deep learning techniques (Long et al., 2015) and detailed human part annotation over the large scale PASCAL dataset (Chen et al., 2014), these difficulties are partially tackled in previous methods. Hariharan et al. (2015) proposed a sequential strategy for object part parsing by first localizing the object with RCNN (Girshick et al., 2014), then segmenting out the human region and finally assigning the pixels inside the human with part

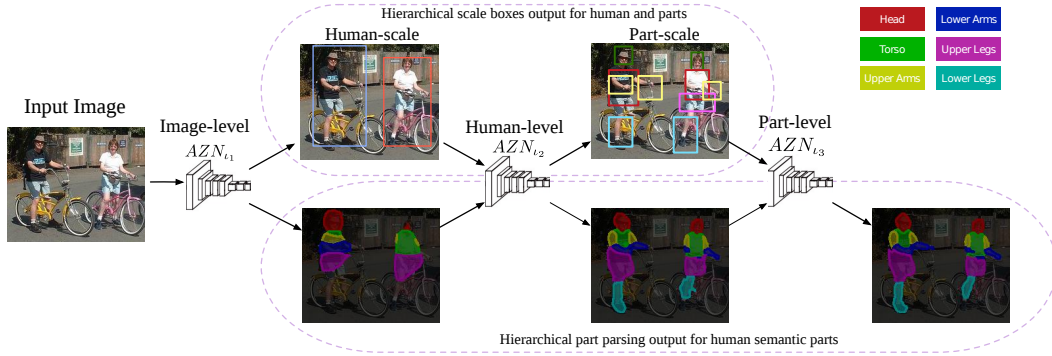


Figure 1: We handle the prediction of human semantic part segmentation in a wild scene scenario. Our proposed AZN refines the part segmentation over three levels of granularity, *i.e.*, image-level (AZN_{l_1}), human-level (AZN_{l_2}), and part-level (AZN_{l_3}). At each level, our AZN outputs both the current parsing potential, and estimated locations and scales for next level of granularity. The part segmentation results gradually become better by taking use of zooming the bounding box proposals.

labels. Wang et al. (2015a) proposed to jointly parse the object and semantic parts, yielding less local confusion and better details in their results. However, these approaches resort to piecewise developing the components, resulting in a relatively complex system, and the variations of part and object scales have not been considered. Motivated by the recent proposal-free end-to-end detection strategies (Huang et al., 2015; Ren et al., 2015; Redmon et al., 2015; Liang et al., 2015), we propose to unify the parsing and scale estimation, yielding a simple and clean method to tackle the difficulties. In fact, we notice that even looking at a local region of the image, the scale of the target object can be directly inferred rather than sampled with multi-scale input images, which is also made possible by the recent end-to-end detection strategies. Thus, the parsing and scale estimation can be unified and mutually beneficial in a single system.

Here, we develop an unified network structure, namely “Auto-Zoom Net” (AZN), based on the fully convolutional neural networks (FCNs) (Long et al., 2015). Our AZN solves the problem of parsing the semantic parts out of all human instances in a natural image, while simultaneously handles the issue of localization and scale estimation. In our network, the parsing potentials are used to automatically discover the locations and scales of human instances. Our model then zooms the image regions based on the estimated locations and scales to refine part segmentation boundaries. This process is iteratively performed and the details of human parts are gradually refined.

1.1 FRAMEWORK

In Fig. 1, we illustrate the testing framework of our approach. Given an input image, our AZN performs over three levels of granularity based on the original image, namely, image-level, human instance-level, and part-level as illustrated in the figure. Specifically, at each level of granularity, our AZN simultaneously outputs the current parsing potential and the estimated locations and scales for the next level of granularity. At the top row, we show the automatically predicted bounding boxes at human level and part level, providing quite accurate localizations of human instances and parts. At the bottom row, we visualize the parsing outputs at each level. The details of human instances and parts are gradually becoming clearer and better by taking use of zooming onto the regions. The output from the final level is used as our parsing result. Last but not the least, our network is unified for both tasks (*i.e.*, part parsing and estimation of locations and scales), yielding an efficient system compared to previous strategies such as the Hypercolumn (Hariharan et al., 2015).

2 BACKGROUNDS

Traditionally, the study of human part parsing has been largely confined to the constrained environments where a human instance in an image is well localized and has a relative simple pose, *e.g.*, standing or walking (Bo & Fowlkes, 2011; Zhu et al., 2011; Eslami & Williams, 2012; Yamaguchi

et al., 2012; Dong et al., 2014; Liu et al., 2015a; Xia et al., 2016). While these works are quite useful given a well cropped human instance like commercial product images, such methods are limited when applied to parsing human in an uncontrolled scenario, as human in real-world images are often in various poses, occluded or highly deformed, which is difficult to be handled by those shape- and appearance-based models with hand-crafted features or bottom-up segments.

Over the past few years, with the powerful semantic segmentation techniques developed based on deep convolutional neural networks (DCNNs) (LeCun et al., 1998) and big data, researchers have made significant performance improvement over object parsing in the wild (Long et al., 2015; Chen et al., 2015a; Dai et al., 2015; Liu et al., 2015b; Noh et al., 2015; Papandreou et al., 2015; Wang et al., 2015b; Zheng et al., 2015; Tsogkas et al., 2015), yielding a strong indication that DCNNs could also parse object into parts in the wild to handle the difficulties of human variations. One can directly apply these deep segmentation models over the whole image, regarding each semantic part as a class label. However, it will suffer from the large scale variation of parts, and many details can easily be missed. Hariharan et al. (2015) proposed to sequentially perform object detection, object parsing and part segmentation, in which the object is first localized by RCNN, then object mask is segmented with a fully convolutional network (FCN) (Long et al., 2015), and finally the part segmentation is performed by partitioning the mask. The sequential process has several drawbacks: first, it is complex to train all components of the model, and second, the error from object masks, *e.g.*, local confusion and inaccurate edges, propagates to the part segments. In order to better localize the details and discover object-level context, Wang et al. (2015a) employed a two-stream FCN to jointly infer object and part segmentations for animals, where the part stream was performed to discover part-level details and the object stream was performed to find object-level context. Although this work can discover object scale context with a fully connect random field, it only used a single scale network for both object and part discovery in potential prediction, where small scale objects might be missed at beginning and the scale variation of parts still remains unsolved.

In fact, in computer vision, tackling the scale issue for better recognition or segmentation has been long studied by considering multiple cues, such as using 3D scene layouts (Hoiem et al., 2008), hierarchical region grouping (Arbelaez et al., 2011; Florack et al., 1996), and applying general or salient object proposals, *e.g.*, (Alexe et al., 2012; Wang et al., 2012). However, most of them used low-level features or only considered constrained scene layouts, which is neither robust in handling wild scene variations nor easily to be unified with DCNNs. To handle the scale issue with DCNNs, researchers commonly use multi-scale side outputs, and perform late fusion, *e.g.*, (Long et al., 2015; Hariharan et al., 2015; Chen et al., 2015a) in order to achieve scale invariance. Most recently, Chen et al. (2015b) proposed a scale attention model, which is a learned spatial combination weights for merging the outputs from three sampled scales. Nonetheless, all these ways are limited by the number of sampled scales that might not be able to cover the right one.

Our “Auto-Zoom Net” model solves these issues by directly regressing the scales for objects and parts, which avoids the sampling error. More importantly, this network is unified with parsing, making the system simple to train and easy to use. Our scale estimation follows the spirit of recent regression for detection networks (Huang et al., 2015; Ren et al., 2015; Redmon et al., 2015), but is further unified with parsing and performs iteratively to handle the part-level details which have not been considered by previous works.

Our model also bears a similarity to recurrent neural networks (Elman, 1990; Hochreiter & Schmidhuber, 1997; Chung et al., 2014), which takes as input the previous prediction. Some recent works have applied recurrent networks for computer vision tasks (Socher et al., 2012; Pinheiro & Collobert, 2013; Byeon et al., 2015). However, none of them iteratively refines the results of human part semantic segmentation by zooming onto the proposed regions.

3 THE AUTO ZOOM NET

In this section, we will introduce the idea of auto-zoom net in detail and formalize the problem, while discussing related algorithms and how auto-zoom net handles variation of scales.

3.1 OBJECTIVES AND THE AUTO ZOOM MODEL.

In the task of image parsing, suppose the provided training examples are $\{\mathbf{I}_i, \mathbf{L}_i\}_{i=1}^n$, where n is the example number, \mathbf{I} is the given image, and \mathbf{L} is the supervision information that provides discrete

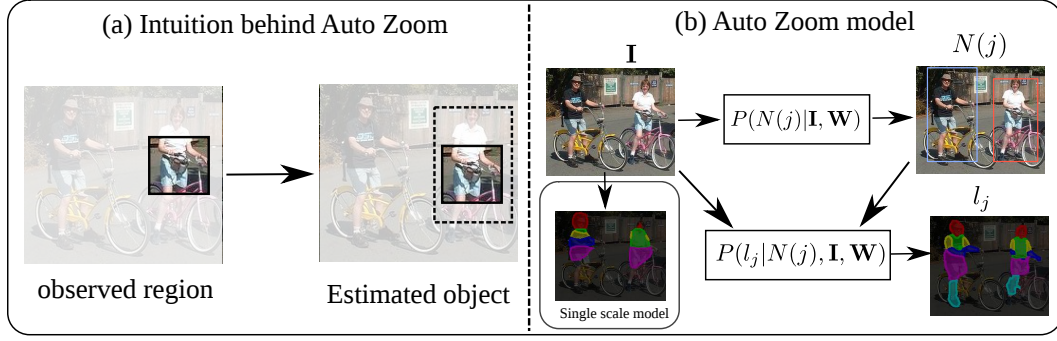


Figure 2: (a) Intuition behind the Auto Zoom model. We can estimate object scale by solely look at a local region. (b) The proposed auto-zoom model predicts the region estimator $N(j)$ for pixel j , and then zooms onto the region to refine the parsing. Details are in Sec. 3.1

semantic labels of interest. By performing supervised learning for parsing, ideally, we wish to learn a structured joint posterior distribution, *i.e.*, $P(\mathbf{L}_i|\mathbf{I}_i, \mathbf{W})$, that can perfectly represent the world. However, it is very difficult to model the high dimensional space. In order to approximate the distribution, researchers commonly decompose the problem by factorizing the distribution into local cliques over pixels or over local regions (superpixels) using random fields with unary-potential and the smooth potentials from neighboring factors.

To be general, we use a pixel as a factorized term for illustration. Particularly, we want to learn a posterior distribution over each pixel j : $P(l_j|N(j), \mathbf{I}, \mathbf{W})$ from an image, where \mathbf{W} is the model parameters and $N(j)$ is a set of selected neighboring pixels w.r.t. j , which is defined so as to be used for both extracting features for learning representation and finding neighbors for message passing. For example, to learn representation, the $N(j)$ for traditional features such as Texton (Shotton et al., 2009) and HOG (Dalal & Triggs, 2005) is a local patch around j , and the neighbor region $N(j)$ for current fully convolutional networks is generally a cropped rectangular region and is determined by the network’s field-of-view centered at j . For passing message in the model, $N(j)$ can represent the locally connected conditional random field Lafferty et al. (2001), or auto-context Tu & Bai (2010). Here, for generality, we unify the notion of local region for both feature representation and message passing.

However, in most of current models, the choice of neighbors, *i.e.*, the spatial factor $N(j)$, is often fixed, either for feature extraction or message passing. Obviously, fixing the field of neighbor for learning or for message passing is not optimal and yields local confusions. On the other hand, changing the field of neighbor can produce significant different results, as shown and explored theoretically by Geiger & Yuille (1991); Lafferty et al. (2001) and practically by many works (Chen et al., 2015a; Krähenbühl & Koltun, 2011). Thus, researchers generally sample multiple scales of input (*i.e.*, vary $N(j)$) and employ either averaging (Chen et al., 2015b) to find the scale stable regions, or selection (Ladicky et al., 2014) to find the best scale output, normally yielding better results.

When predicting over a natural image, as illustrated in Fig. 2 (a), even by looking at a truncated region from an object in images, we can estimate the object scale. Thus, rather than sampling $N(j)$ without any priori knowledge, we can actually estimate it by regarding it as another hidden factor in a probabilistic model, *i.e.*, $P(N(j)|\mathbf{I}, \mathbf{W})$. Intuitively, if $N(j)$ for learning representation is always correctly estimated (*i.e.*, the target objects are always in the same scale), the final representation in the feature space will be clustered denser, which is known to benefit statistical learning. Thus our proposed probabilistic model becomes:

$$\begin{aligned}
 P(l_j|\mathbf{I}, \mathbf{W}) &= \int_{N(j)} P(l_j, N(j)|\mathbf{I}, \mathbf{W}); \\
 P(l_j, N(j)|\mathbf{I}, \mathbf{W}) &= P(l_j|N(j), \mathbf{I}, \mathbf{W})P(N(j)|\mathbf{I}, \mathbf{W});
 \end{aligned} \tag{1}$$

we call this model as auto-zoom net to find the neighborhood either for feature representation or message passing. To learn such a model, one may conduct the Expectation-Maximization (EM) algorithm to maximize the expected complete-data log-likelihood, *i.e.*,

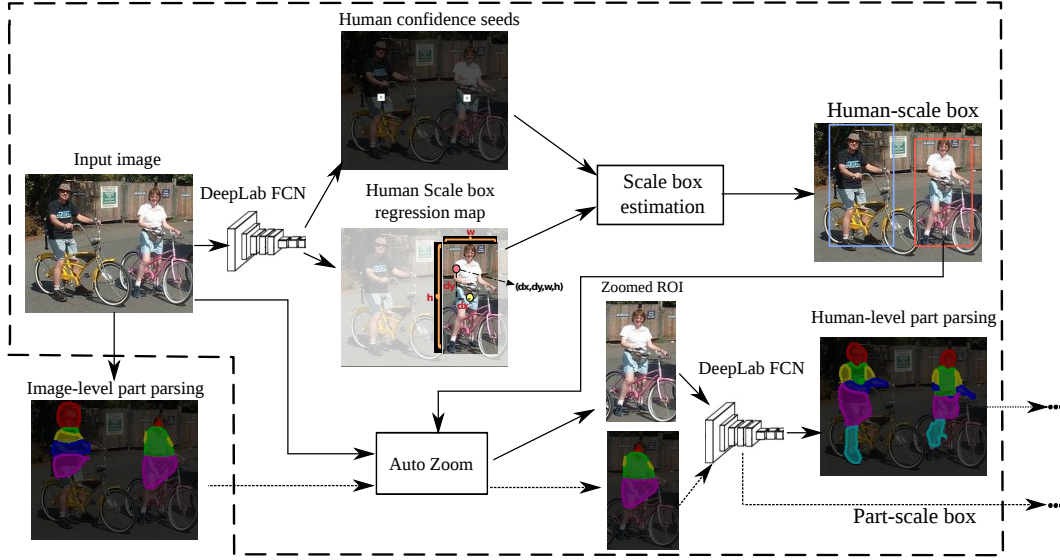


Figure 3: Detailed structure for Auto-Zoom model, which is correspondent to the probabilistic model in Fig. 2. The solid line indicates a single level AZN (details are presented Sec. 3.2), and the dashed line indicates extra input and output for hierarchical AZN (details in Sec. 3.3). (best viewed in color)

$E_{P(N(j)|\mathbf{R}_j, \mathbf{W})}(\log P(l_j, N(j)|\mathbf{I}, \mathbf{W}))$ in order to estimate $N(j)$, where \mathbf{R}_j is the bounding box region for neighborhood estimation. In our parsing tasks, the correct parsing scale can be directly retrieved by drawing a bounding box over the annotated regions which is served as a supervision for learning the probability, *i.e.*, $P(N(j)|\mathbf{R}_j, \mathbf{W})$, while this information is rarely considered by previous DCNN parsing works.

Actually, the previous multi-scale sampling models can easily be understood in this model, where we average over the sampled $N(j)$ for roughly approximation of the marginal distributions, *i.e.*, $\sum_s P(l_j, N(j)_s|\mathbf{I}, \mathbf{W})/|S| \rightarrow P(l_j|\mathbf{I}, \mathbf{W})$, where $|S|$ is the number of sampled scales. However, we argue that by predicting $N(j)$, the label estimation can be even more accurate. In practice, directly estimating the object scale in DCNNs has also been discussed in works for object detections or related fields (Hariharan et al., 2015; Dai et al., 2015; Ren et al., 2015; Redmon et al., 2015; Huang et al., 2015; Kar et al., 2015), while this work provides a more general view to understand it based on a perspective of neighborhood connection in a Bayesian graphical model.

3.2 AUTO ZOOM NET FOR PARSING HUMAN IN THE WILD.

To construct the model in Eqn. (1), we need to learn the models for predicting pixel j , *i.e.*, $P(l_j|N(j))$ and $P(N(j))$, where we omit \mathbf{I}, \mathbf{W} in the condition to simplify the notations. Specifically, for human parsing tasks, as illustrated in Fig. 2 (b), the auto-zoom net first predicts the object scale, *i.e.*, $N(j)$, and takes it as conditional information for representing human parts feature, which makes the inference of each pixel for human instances under a proper scale, *i.e.*, with $P(l_j|N(j))$, yielding a much better results compared to a single model without scale handling.

As presented at Sec. 1.1, both of the probabilistic models (*i.e.*, $P(l_j|N(j))$ and $P(N(j))$) are built on the state-of-art FCN (Long et al., 2015) which is trained on the ImageNet data (Russakovsky et al., 2015). Such a model provides high robustness to object variations. The technique details with those two proposed models are visualized in Fig. 3, which includes both training and testing phases for learning the distributions.

Training and Testing phases. We utilize a modern version of the FCN network structures proposed by Chen et al. (2015a), namely the **DeepLab-LargeFOV** to be our learning models. Gener-

ally, it takes as input an image and a pixel-wise annotated label map. We refer readers to the original paper for details due to the space limits.

As shown at the dashed curved part of Fig. 3, $P(N(j))$ and $P(l_j|N(j))$ are actually performed by two networks sharing the same structure. The first network is a scale estimator network (SEN) used to estimate the $N(j)$ for each pixel in terms of correspondent proper object scale. The second network takes the estimated scale, and then zooms onto the region of interest for better inference.

For training the SEN, *i.e.*, $P(N(j))$ for each pixel, in practice, we transfer the learning of $N(j)$ to the learning of object scales, we will discuss how to reversely infer $N(j)$ at testing stage. Specifically, for learning, we design two kinds of output label maps for object scales, as visualized at right top of Fig. 3. The first one is bounding boxes, and it represents the regions of interest. In particular, we use a four-channel output for each pixel, *i.e.*, $\mathbf{l}_{bj} = \{dx_j, dy_j, h_j, w_j\}$, yielding a label map \mathbf{L}_b . The second one is the confidence seeds map where a set of seed regions are located at the center region of each human instance. These center points can estimate the object scale better than the other points at region boundary, since it is easier to localize the object with center points than points at boundaries, as indicated by Huang et al. (2015). We use $l_{cj} \in \{0, 1\}$ and $\mathbf{l}_{cj} = 1$ indicates j is at the seed. Formally, the confidence map can be represented as \mathbf{L}_c . Then, given the human segmentation ground truth label map, it is easy for us to derive the training examples from the human segment label maps, $\mathcal{H} = \{\mathbf{I}_i, \mathbf{L}_{bi}, \mathbf{L}_{ci}\}_{i=1}^n$, and n is the training instance number. Finally, we minimize the negative log likelihood for the FCN model, and the loss of the SEN is defined as:

$$\begin{aligned} l_{SEN}(\mathcal{H}|\mathbf{W}) &= \frac{1}{N} \left(\sum_i (l_b(\mathbf{I}_i, \mathbf{L}_{bi}|\mathbf{W}) + \lambda l_c(\mathbf{I}_i, \mathbf{L}_{ci}|\mathbf{W})) \right); \\ \text{where, } l_b(\mathbf{I}, \mathbf{L}_b|\mathbf{W}) &= -\beta \sum_{j:l_{cj}=1} \log P(l_{cj}^* = 1|\mathbf{I}, \mathbf{W}) - (1 - \beta) \sum_{j:l_{cj}=0} \log P(l_{cj}^* = 0|\mathbf{I}, \mathbf{W}); \\ l_c(\mathbf{I}, \mathbf{L}_c|\mathbf{W}) &= \frac{1}{|\mathbf{L}_{cj}^+|} \sum_{j:l_{cj}=1} \|\mathbf{l}_{bj} - \mathbf{l}_{bj}^*\|_2; \end{aligned} \quad (2)$$

For the confidence seeds, we employ the balanced cross entropy loss, where the l_{cj}^* and l_{cj} are the predicted value and ground truth value respectively. The probability is from a sigmoid function performing on the activation of last layer of CNN at pixel j . β is defined as the portion of $l_{cj} = 0$ in the image, which is used to balance the positive and negative instances. The loss for generating scale box is the Euclidean distance over the confidence seeds points, and $|\mathbf{L}_{cj}^+|$ is the number of $l_{cj} = 1$.

During testing, the SEN can output both the confidence seed potential $P(l_{cj}^* = 1|\mathbf{I}, \mathbf{W})$ and a 4 dimension scale box \mathbf{l}_{bj}^* for each pixel j . We regard the each seed with potential higher than 0.5 to be reliable and output a scale box. We perform non-maximum suppression based on the confidence potentials, yielding several scale boxes as candidate regions with confidence scores, *i.e.*, $P(\mathbf{b}_k)$.

Technically, in the case of feature extraction from CNN, one way of using $N(j)$ for each pixel is through cropping and pooling over feature maps, similar to Faster RCNN (Ren et al., 2015), which adapts $N(j)$ to the region of interest (ROI) for classification. In parsing tasks, we regard $N(j)$ as a region dependent on the size of the covered scale box, formally, $N(j) = f(w_j, h_j)N(j)_o$ where w_j, h_j are the width and height of the box, $f()$ is a factor computed from the box and $N(j)_o$ is the original scale of the network. We will discuss $f(w, h)$ in detail at Sec. 4.1. Thus, this is actually a zooming operation of $N(j)$ for the ROI inside the detected box, as visualized at bottom row of Fig. 3. For the pixels not covered, we keep the $N(j)$ unchanged. Sometimes, the boxes can overlap with each other, which give us multiple $N(j)$ for the pixel in the overlapping regions. We denote multiple fields for j as $\{N(j)_s\}_{s=1}^{n_s}$, and set their probability to be the normalized confidence score $P(N(j)_s) = P(\mathbf{b}_s) / \sum_s P(\mathbf{b}_s)$.

For training the model of semantic parsing potential given $N(j)$, *i.e.* $P(l_j|N(j))$, we need to first train a FCN parsing model in original image scale, and then we additionally train another FCN model based on all the zoomed images regions, with given ground truth label maps $\mathcal{H}_p = \{\mathbf{L}_{pi}\}_{i=1}^n$. In our case, the FCN parsing model in original image scale has the same structure as the SEN discussed above. Thus, we merge this part with the SEN training, yielding the loss of our single level AZN:

$$l_{AZN}(\mathcal{H}, \mathcal{H}_p|\mathbf{W}) = \frac{1}{N} \sum_i l_p(\mathbf{I}_i, \mathbf{L}_{pi}) + l_{SEN}(\mathcal{H}|\mathbf{W}); \quad (3)$$

where $l_p(\mathbf{I}_i, \mathbf{L}_{pi})$ is the commonly used multinomial logistic regression loss for classification.

For testing the auto zoom model, we can first run a single scale AZN, yielding scale boxes and single scale parsing potentials, and then we zoom onto scale boxes and parse these regions based on the second FCN model. Finally, by combining the two parsing outputs, we can get our final results. Formally, based on Eqn. 1, we have $P(l_j|\mathbf{I}, \mathbf{W}) = \sum_s P(l_j|N(j)_s)P(N(j)_s)$.

3.3 HIERARCHICAL AUTO ZOOM NET.

To estimate detailed regions like human part parsing, it has certain difficulties even given the human scale, since human part itself also contains large scale variations, *e.g.*, body, head, arm and hand. Here, we further develop the hierarchical auto-zoom net (HAZN), which concatenates the auto-zoom model to handle multi-level scales issues as introduced at the framework *i.e.*, Fig. 1. The output from the previous level will be served as a prior message for the current level for scale estimation.

Formally, the hierarchical auto zoom net generalizes the formulation in Eqn. (1) from $P_\iota(l_j|N(j)_\iota)$ to $P_\iota(l_j, N(j)_\iota|N(j)_{\iota-1}, P_{\iota-1}(l_j|N(j)_{\iota-1}))$, where ι is the level of interest in the hierarchical model. It depends on the scale estimation and parsing result from the previous level $\iota - 1$. Note that one can product all the conditional distributions to get the joint distribution of the HAZN. By formulating in this way, it actually unifies the structures of SEN and parsing net in our single level AZN in Sec. 3.2, where both of them take as input the image and potentials from the previous level, and output the scale estimator and potentials for next level, except the first and last level in the hierarchy.

In practice, to combine potential maps from the last level of HAZN, we also zoom the respective regions inferred from $N(j)$, then concatenate it to the final score layer of the FCN, and finally learn a 5×5 kernel to re-predict the potentials, yielding a potential conditioned on the message from the last level.

4 EXPERIMENTS

4.1 IMPLEMENT DETAILS

In our HAZN, to get the confidence seeds of parts ground truth, we select central 7×7 pixels within each part segments. For human, we also take use of the human instance mask from the PASCAL part data set (Chen et al., 2014).

To determine the optimum zoom ratio for a human proposal, *i.e.*, $f(w, h)$ in the function $N(j) = f(w_j, h_j)N(j)_o$ (see Sec. 3.2), where w_j, h_j are the width and height of the scale box and $N(j)_o$ is the original scale of the network. We employ different strategies for the human level and the part level. For part level, $f(w_j, h_j)_p = \max(w_j, h_j)/s_p$, and $s_p = 255$ is the optimal zoom scale in our case. For human level, since we perform our experiments in PASCAL human class, there are many cases that a human instance is largely truncated, while the upper body of a human is often visible. To handle this, suppose a human box has size of $[w_{j1}, h_{j1}]$, and upper body is $[w_{j2}, h_{j2}]$. In order to estimate the human scale for $N(j)$ transformation, we set $f(w_j, h_j)_h = \max(\max(w_{j1}, h_{j1})/s_h, \max(w_{j2}, h_{j2})/s_u)$, where $s_h = 280, s_u = 140$ are the optimal zoom scales for human and upper body respectively. This allows us to trust upper body box when a human is heavily occluded. We validate all the part and body scale parameters s_p, s_h, s_u based on a validation set. For dealing with the extreme cases, when only human head is visible, we further constrain the range of zoom scale, *i.e.*, $f(w_j, h_j)_h \in [0.4, 2]$.

4.2 EXPERIMENTAL PROTOCOL

Training Stochastic Gradient Descent with mini-batch is used for training. We set mini-batch size of 30 images and initial learning rate of 0.001 (0.01 for the final classifier layer). The learning rate is multiplied by 0.1 after every 2000 iterations. We use momentum of 0.9 and weight decay of 0.0005. Fine-tuning our network on all the reported experiments takes about 30 hours on a NVIDIA Tesla K40 GPU. The average inference time for one PASCAL image is 1300 ms/image.

Evaluation metric The segmentation performance is measured in terms of pixel intersection-over-union (IOU) averaged across classes (Everingham et al., 2014). The quality of bounding box proposals for human and human parts is measured by average precision (AP).

Dataset We conduct experiments on the dataset annotated by (Chen et al., 2014) from PASCAL VOC 2010 dataset. Wang & Yuille (2015); Wang et al. (2015a) have worked on the animal part segmentation for the dataset. On the other hand, we focus on the *person* part, which has larger variation in scale and pose than other human parsing datasets (Wang et al., 2007; Yamaguchi et al., 2012). The dataset contains detailed part annotations for every person, including head, torso, *etc.* We merge the annotations to be Head, Torso, Upper/Lower Arms and Upper/Lower Legs, resulting in six person part classes and one background class. We only use those images containing persons for training (1716 images) and validation (1817 images).

Network architecture We use DeepLab-LargeFOV as building blocks in our proposed HAZN. HAZN performs three levels of granularity based on the input image: image scale, human instance scale, and part scale. At each stage, HAZN outputs both part parsing potentials and estimated locations and scales for the next level of granularity. Note that the simplest HAZN with only one granularity (*i.e.*, image scale) is DeepLab-LargeFOV.

4.3 EXPERIMENTAL RESULTS

Importance of each level of granularity As shown in Tab. 1, we experiment with the effect of reducing the levels of granularity of proposed HAZN. Our proposed HAZN with three levels of granularity (image scale, human scale, and part scale) attains the performance of 56.11%, which is 4.3% better than the baseline DeepLab-LargeFOV (which exploits only image scale). We denote as “HAZN (no part scale)” when removing AZN-Part from our full model and as “HAZN (no human scale)” when removing AZN-Human from our full model. It turns out that removing the part scale or human scale from the HAZN full model results in 1.3% performance degradation, but still yields 3% improvement over the baseline. As a result, it is crucial for HAZN to exploit all three levels of granularity to achieve the best performance. We have also compared with another baseline, DeepLab-LargeFOV-CRF, which employs a fully connected Conditional Random Field (CRF) (Krähenbühl & Koltun, 2011) as post processing (Chen et al., 2015a) to refine the object boundary, which is commonly used for general object semantic segmentation (*i.e.*, no part segmentation). The resulting performance is 3.2% worse than our HAZN (full model). The reason is that since the fully connected CRF requires bilateral kernels (Adams et al., 2010) for fast inference, it is difficult to recover the human part boundaries with features, such as position and color intensity. On the other hand, our HAZN is more effective on the part segmentation task.

| Method | head | torso | u-arms | l-arms | u-legs | l-legs | bg | Avg |
|-----------------------|-------|-------|--------|--------|--------|--------|-------|-------|
| DeepLab-LargeFOV | 78.09 | 54.02 | 37.29 | 36.85 | 33.73 | 29.61 | 92.85 | 51.78 |
| DeepLab-LargeFOV-CRF | 80.13 | 55.56 | 36.43 | 38.72 | 35.50 | 30.82 | 93.52 | 52.95 |
| HAZN (no part scale) | 79.65 | 57.56 | 40.62 | 40.45 | 37.72 | 34.32 | 93.31 | 54.80 |
| HAZN (no human scale) | 80.25 | 57.20 | 42.24 | 42.02 | 36.40 | 31.96 | 93.42 | 54.78 |
| HAZN (full model) | 80.79 | 59.11 | 43.05 | 42.76 | 38.99 | 34.46 | 93.59 | 56.11 |

Table 1: Segmentation accuracy (%) on PASCAL-Person-Part in terms of mean pixel IOU. DeepLab-LargeFOV is the simplest case of HAZN when employing only one level of granularity. We experiment with removing the levels of granularity of proposed HAZN. We also compare with DeepLab-LargeFOV-CRF which employs a fully connected CRF as post processing.

Qualitative results We show some human part semantic segmentation results on the validation set in Fig. 5. The baseline DeepLab-LargeFOV usually yields noisy blob-like results, and cannot detect the parts for small scale human instances. Employing a fully connected CRF simply smoothes the segmentation results slightly. Our HAZN (no part scale) is able to detect the small scale human instances and further produces correspondingly reasonable part segmentation results, while our HAZN (no human scale) helps refine the part boundaries (by zooming the part proposals) especially for the lower legs. Finally, our HAZN (full model) attains the best visual results by exploiting both human and part scales.

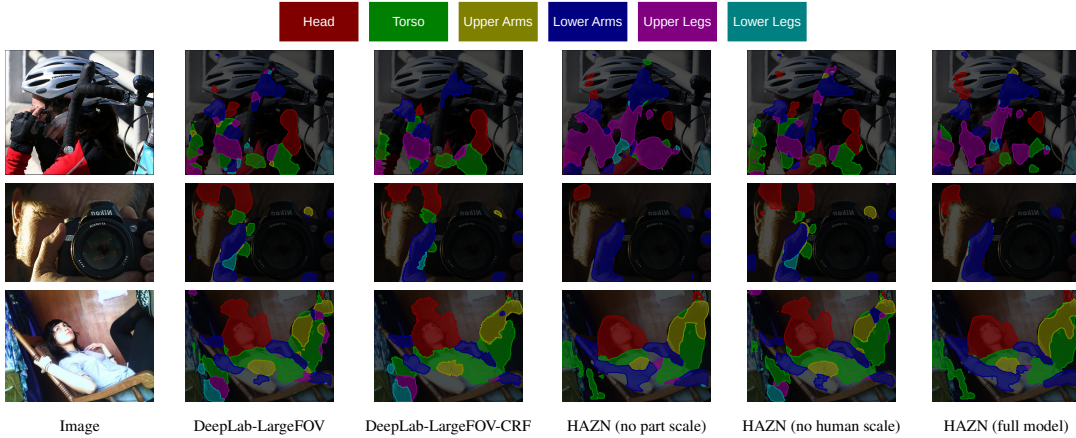


Figure 4: Failure modes: qualitative results for our proposed models and baselines. Our models suffer from the heavy occlusion and challenging poses.

Failure modes We show some visual results for our failure modes in Fig. 4. We find that our models have difficulty in segmenting the parts for human instances with heavy occlusion and with challenging poses.

Segmentation accuracy across human instance scales HAZN exploits different levels of granularity for human part segmentation. Here, we are interested in understanding the improvement of segmentation accuracy induced by HAZN across different scales of human instances. We categorize all the groundtruth human instances into four scales according to the bounding box size s_b (the square root of bounding box area), and compute the mean pixel IOU (within ground-truth bounding box) for each scale respectively. The four scales for human instances are defined by the following criteria: (1) scale XS: $s_b \in [20, 80]$, where the human scale is extremely small; (2) scale S: $s_b \in [80, 140]$; (3) scale M: $s_b \in [140, 220]$; (4) scale L: $s_b \in [220, 520]$, where usually only the head or torso of the large-scale human is visible. The results are reported in Tab. 2. We find that the baseline DeepLab-LargeFOV fails to detect human parts at scale XS or S (usually only the head or the torso can be detected), while our HAZN (full model) improves over it significantly by 13% for scale XS and 8.4% for scale S, which demonstrates the effectiveness of our proposed method to handle the variation of human scales. We find that employing a fully connected CRF is not effective for segmenting the parts of small scale instances, and it slightly improves the performance for large scale instances. However, the improvement is still not as effective as our HAZN. Moreover, our HAZN (no part scale) performs better than HAZN (no human scale) at scale XS, while worse at scale M. It shows that for small scale instances, it is better to zoom the human bounding box proposals, and for median scale instances, it is better to zoom the part bounding box proposals. Our HAZN (full model) attains the best performance by taking use of both human and part proposals.

| Method | XS | S | M | L |
|-----------------------|------|------|------|------|
| DeepLab-LargeFOV | 32.5 | 44.5 | 50.7 | 50.9 |
| DeepLab-LargeFOV-CRF | 31.5 | 44.6 | 51.5 | 52.5 |
| HAZN (no part scale) | 43.5 | 50.6 | 52.9 | 53.4 |
| HAZN (no human scale) | 38.2 | 51.0 | 55.1 | 53.4 |
| HAZN (full model) | 45.5 | 52.9 | 54.9 | 54.6 |

Table 2: Within-bounding-box scale-wise segmentation accuracy (%) on PASCAL-Person-Part in terms of mean pixel IOU.

Evaluation of part bounding box proposals In the last level of granularity (*i.e.*, part scale), HAZN exploits bounding box proposals for part segmentation refinement. It is thus interesting to evaluate our part bounding box proposals. The results in terms of AP are reported in Tab. 3. We

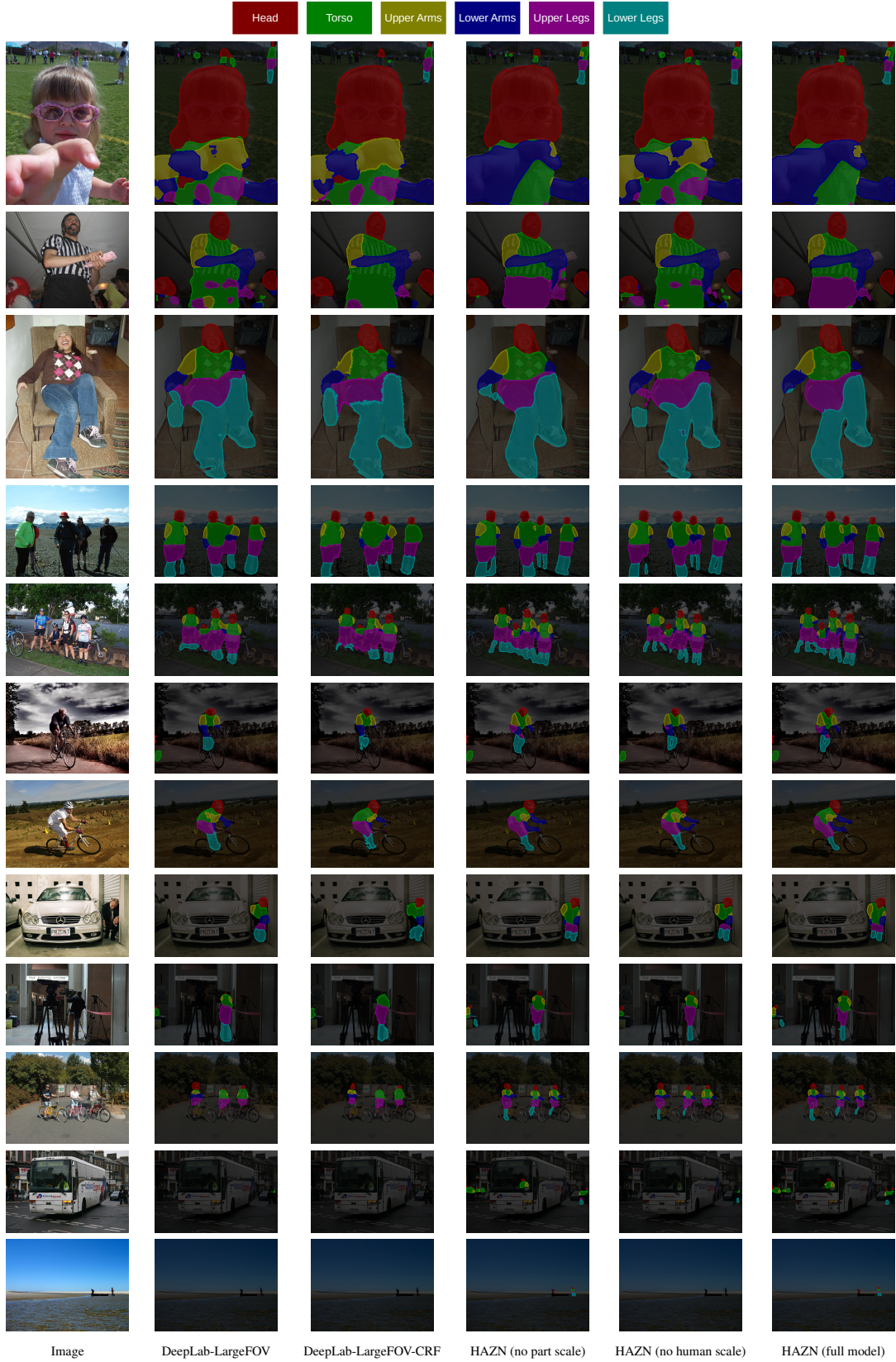


Figure 5: Qualitative comparison between our proposed models and baselines. Employing a fully connected CRF (DeepLab-LargeFOV-CRF) is not effective in part segmentation, which simply smoothes the results by DeepLab-LargeFOV. On the other hand, our proposed HAZN models attain better visual segmentation results, especially for small scale human instances.

set the part bounding box IOU threshold to 0.3 in all our experiments so that the part recall rates are higher for the following refinement. As shown in the table, we find that HAZN (full model) significantly outperforms HAZN with (no human scale) by 10.7%, and it consistently improves over all part categories. Furthermore, employing our scale zooming strategy is essential to attain high AP. The performance drops a lot by 6% if zooming strategy is not employed.

| Method | head | torso | u-arms | l-arms | u-legs | l-legs | mAP |
|-----------------------------|-------|-------|--------|--------|--------|--------|-------|
| HAZN (no human scale) | 48.34 | 28.95 | 27.39 | 20.98 | 22.40 | 12.05 | 26.69 |
| HAZN (full model - zooming) | 55.86 | 35.10 | 29.36 | 23.82 | 27.22 | 16.78 | 31.35 |
| HAZN (full model) | 69.16 | 44.35 | 37.43 | 24.11 | 31.90 | 17.51 | 37.41 |

Table 3: Average Precision (%) for human part bounding box proposals on PASCAL-Person-Part. The bounding box IOU threshold is set to 0.3.

Evaluation of human bounding box proposals For the human bounding box proposals, we consider that a human instance is detected if there is one proposal that has at least 40% bounding box overlap with it in terms of IOU. On the validation set, we attain AP = 45.51%.

5 CONCLUSIONS

In this paper, we propose the “Auto-Zoom Net” (AZN) to parse human in the wild, which is a robust and unified network with scale issue aware and tackled simultaneously. Our network performs better than the previous state-of-art deep parsing strategies for part segmentation, especially for instances and parts at small scale. We hope that our work inspires others to perform further research on automatic scale handling that can be widely applied to other vision tasks.

In the future, for the AZN model, we would love to first better explore the dense distribution of $P(N(j)|\mathbf{I}, \mathbf{W})$ in Eqn. (1), where the field of view for each pixel j can be optimized, rather than assigned using bounding box model. In addition, we can also explore the message passing based on the predicted scales $N(j)$, and long term memory model that combines multiple levels of outputs. Later, further progress can be made by applying AZN to combine other tasks such as 3D pose estimation for regularization (Xia et al., 2016), depth estimation of instances as scale is closely related with distance (Ladicky et al., 2014) and parsing human into even more details, such as hand, foot, and eyes.

REFERENCES

- Adams, Andrew, Baek, Jongmin, and Davis, Myers Abraham. Fast high-dimensional filtering using the permutohedral lattice. In *Eurographics*, 2010.
- Alexe, Bogdan, Deselaers, Thomas, and Ferrari, Vittorio. Measuring the objectness of image windows. *PAMI.*, 34(11):2189–2202, 2012.
- Arbelaez, Pablo, Maire, Michael, Fowlkes, Charless, and Malik, Jitendra. Contour detection and hierarchical image segmentation. *PAMI*, 33(5):898–916, 2011.
- Bo, Yihang and Fowlkes, Charless C. Shape-based pedestrian parsing. In *CVPR*, 2011.
- Byeon, Wonmin, Breuel, Thomas M, Raue, Federico, and Liwicki, Marcus. Scene labeling with lstm recurrent neural networks. In *CVPR*, 2015.
- Chen, Liang-Chieh, Papandreou, George, Kokkinos, Iasonas, Murphy, Kevin, and Yuille, Alan L. Semantic image segmentation with deep convolutional nets and fully connected crfs. In *ICLR*, 2015a.
- Chen, Liang-Chieh, Yang, Yi, Wang, Jiang, Xu, Wei, and Yuille, Alan L. Attention to scale: Scale-aware semantic image segmentation. *arXiv:1511.03339*, 2015b.

- Chen, Xianjie, Mottaghi, Roozbeh, Liu, Xiaobai, Fidler, Sanja, Urtasun, Raquel, and Yuille, Alan L. Detect what you can: Detecting and representing objects using holistic models and body parts. In *CVPR*, 2014.
- Chung, Junyoung, Gulcehre, Caglar, Cho, KyungHyun, and Bengio, Yoshua. Empirical evaluation of gated recurrent neural networks on sequence modeling. *arXiv:1412.3555*, 2014.
- Dai, Jifeng, He, Kaiming, and Sun, Jian. Boxsup: Exploiting bounding boxes to supervise convolutional networks for semantic segmentation. In *ICCV*, 2015.
- Dalal, Navneet and Triggs, Bill. Histograms of oriented gradients for human detection. In *CVPR*, pp. 886–893, 2005.
- Dong, Jian, Chen, Qiang, Shen, Xiaohui, Yang, Jianchao, and Yan, Shuicheng. Towards unified human parsing and pose estimation. In *CVPR*, 2014.
- Elman, Jeffrey L. Finding structure in time. *Cognitive science*, 14(2):179–211, 1990.
- Eslami, S. M. Ali and Williams, Christopher K. I. A generative model for parts-based object segmentation. In *NIPS*, 2012.
- Everingham, Mark, Eslami, SM Ali, Gool, Luc Van, Williams, Christopher KI, Winn, John, and Zisserman, Andrew. The pascal visual object classes challenge: A retrospective. *IJCV*, 111(1): 98–136, 2014.
- Florack, Luc, Romeny, Bart Ter Haar, Viergever, Max, and Koenderink, Jan. The gaussian scale-space paradigm and the multiscale local jet. *IJCV*, 18(1):61–75, 1996.
- Geiger, Davi and Yuille, Alan L. A common framework for image segmentation. *IJCV*, 6:227–243, 1991.
- Girshick, Ross, Donahue, Jeff, Darrell, Trevor, and Malik, Jagannath. Rich feature hierarchies for accurate object detection and semantic segmentation. In *CVPR*, 2014.
- Hariharan, Bharath, Arbeláez, Pablo, Girshick, Ross, and Malik, Jitendra. Hypercolumns for object segmentation and fine-grained localization. In *CVPR*, 2015.
- Hochreiter, Sepp and Schmidhuber, Jürgen. Long short-term memory. *Neural computation*, 9(8): 1735–1780, 1997.
- Hoiem, Derek, Efros, Alexei A., and Hebert, Martial. Putting objects in perspective. *IJCV*, 80(1): 3–15, 2008.
- Huang, Lichao, Yang, Yi, Deng, Yafeng, and Yu, Yinan. Densebox: Unifying landmark localization with end to end object detection. *arXiv:1509.04874*, 2015.
- Kar, Abhishek, Tulsiani, Shubham, Carreira, João, and Malik, Jitendra. Amodal completion and size constancy in natural scenes. *CoRR*, abs/1509.08147, 2015.
- Krähenbühl, Philipp and Koltun, Vladlen. Efficient inference in fully connected crfs with gaussian edge potentials. In *NIPS*, 2011.
- Ladicky, Lubor, Shi, Jianbo, and Pollefeys, Marc. Pulling things out of perspective. In *2014 IEEE Conference on Computer Vision and Pattern Recognition, CVPR 2014, Columbus, OH, USA, June 23-28, 2014*, pp. 89–96, 2014.
- Lafferty, John D., McCallum, Andrew, and Pereira, Fernando C. N. Conditional random fields: Probabilistic models for segmenting and labeling sequence data. In *ICML*, pp. 282–289, 2001.
- LeCun, Yann, Bottou, Léon, Bengio, Yoshua, and Haffner, Patrick. Gradient-based learning applied to document recognition. *Proceedings of the IEEE*, 86(11):2278–2324, 1998.
- Liang, Xiaodan, Wei, Yunchao, Shen, Xiaohui, Yang, Jianchao, Lin, Liang, and Yan, Shuicheng. Proposal-free network for instance-level object segmentation. *CoRR*, abs/1509.02636, 2015.

- Lin, Tsung-Yi, Maire, Michael, Belongie, Serge, Hays, James, Perona, Pietro, Ramanan, Deva, Dollár, Piotr, and Zitnick, C Lawrence. Microsoft coco: Common objects in context. In *ECCV*, 2014.
- Liu, Si, Liang, Xiaodan, Liu, Luoqi, Shen, Xiaohui, Yang, Jianchao, Xu, Changsheng, Lin, Liang, Cao, Xiaochun, and Yan, Shuicheng. Matching-cnn meets knn: Quasi-parametric human parsing. In *CVPR*, 2015a.
- Liu, Ziwei, Li, Xiaoxiao, Luo, Ping, Loy, Chen Change, and Tang, Xiaoou. Semantic image segmentation via deep parsing network. In *ICCV*, 2015b.
- Long, Jonathan, Shelhamer, Evan, and Darrell, Trevor. Fully convolutional networks for semantic segmentation. In *CVPR*, 2015.
- Noh, Hyeonwoo, Hong, Seunghoon, and Han, Bohyung. Learning deconvolution network for semantic segmentation. *arXiv:1505.04366*, 2015.
- Papandreou, George, Chen, Liang-Chieh, Murphy, Kevin, and Yuille, Alan L. Weakly- and semi-supervised learning of a dcnn for semantic image segmentation. In *ICCV*, 2015.
- Pinheiro, Pedro HO and Collobert, Ronan. Recurrent convolutional neural networks for scene parsing. *arXiv:1306.2795*, 2013.
- Redmon, Joseph, Divvala, Santosh Kumar, Girshick, Ross B., and Farhadi, Ali. You only look once: Unified, real-time object detection. *CoRR*, abs/1506.02640, 2015.
- Ren, Shaoqing, He, Kaiming, Girshick, Ross, and Sun, Jian. Faster r-cnn: Towards real-time object detection with region proposal networks. *arXiv:1506.01497*, 2015.
- Russakovsky, Olga, Deng, Jia, Su, Hao, Krause, Jonathan, Satheesh, Sanjeev, Ma, Sean, Huang, Zhiheng, Karpathy, Andrej, Khosla, Aditya, Bernstein, Michael, Berg, Alexander C., and Fei-Fei, Li. ImageNet Large Scale Visual Recognition Challenge. *IJCV*, pp. 1–42, 2015.
- Shotton, Jamie, Winn, John M., Rother, Carsten, and Criminisi, Antonio. Textonboost for image understanding: Multi-class object recognition and segmentation by jointly modeling texture, layout, and context. *IJCV*, 81(1):2–23, 2009.
- Socher, Richard, Huval, Brody, Bath, Bharath, Manning, Christopher D, and Ng, Andrew Y. Convolutional-recursive deep learning for 3d object classification. In *NIPS*, 2012.
- Tsogkas, Stavros, Kokkinos, Iasonas, Papandreou, George, and Vedaldi, Andrea. Semantic part segmentation with deep learning. *arXiv:1505.02438*, 2015.
- Tu, Zhuowen and Bai, Xiang. Auto-context and its application to high-level vision tasks and 3d brain image segmentation. *IEEE Trans. Pattern Anal. Mach. Intell.*, 32(10):1744–1757, 2010.
- Wang, Jianyu and Yuille, Alan. Semantic part segmentation using compositional model combining shape and appearance. In *CVPR*, 2015.
- Wang, Liming, Shi, Jianbo, Song, Gang, and Shen, I-Fan. Object detection combining recognition and segmentation. In *ACCV*. 2007.
- Wang, Peng, Wang, Jingdong, Zeng, Gang, Feng, Jie, Zha, Hongbin, and Li, Shipeng. Salient object detection for searched web images via global saliency. In *CVPR*, pp. 3194–3201, 2012.
- Wang, Peng, Shen, Xiaohui, Lin, Zhe, Cohen, Scott, Price, Brian, and Yuille, Alan. Joint object and part segmentation using deep learned potentials. In *ICCV*, 2015a.
- Wang, Peng, Shen, Xiaohui, Lin, Zhe, Cohen, Scott, Price, Brian, and Yuille, Alan L. Towards unified depth and semantic prediction from a single image. In *CVPR*, 2015b.
- Xia, Fangting, Zhu, Jun, Wang, Peng, and Yuille, Alan L. Pose-guided human parsing with deep learned features. *AAAI*, abs/1508.03881, 2016.

- Yamaguchi, Kota, Kiapour, M Hadi, Ortiz, Luis E, and Berg, Tamara L. Parsing clothing in fashion photographs. In *CVPR*, 2012.
- Zhang, Ning, Donahue, Jeff, Girshick, Ross, and Darrell, Trevor. Part-based r-cnns for fine-grained category detection. In *ECCV*. 2014.
- Zheng, Shuai, Jayasumana, Sadeep, Romera-Paredes, Bernardino, Vineet, Vibhav, Su, Zhizhong, Du, Dalong, Huang, Chang, and Torr, Philip. Conditional random fields as recurrent neural networks. In *ICCV*, 2015.
- Zhu, Long Leo, Chen, Yuanhao, Lin, Chenxi, and Yuille, Alan. Max margin learning of hierarchical configural deformable templates (hcdts) for efficient object parsing and pose estimation. *IJCV*, 93(1):1–21, 2011.